Petroleum Science 19 (2022) 1347–1360

Contents lists available at ScienceDirect

Petroleum Science

journal homepage: www.keaipublishing.com/en/journals/petroleum-science

Experimental investigation of erosion rate for gas-solid two-phase flow in 304 stainless /L245 carbon steel

Bingyuan Hong [a, b], Yanbo Li [b], Xiaoping Li [b, *], Gen Li [c], Andong Huang [d], Shuaipeng Ji [b], Weidong Li [e], Jing Gong [b, **], Jian Guo [a]

[a] National-Local Joint Engineering Laboratory of Harbor Oil & Gas Storage and Transportation Technology, Zhejiang Provincial Key Laboratory of Petrochemical Pollution Control, Zhejiang Ocean University, Zhoushan, 316022, PR China
[b] National Engineering Laboratory for Pipeline Safety, MOE Key Laboratory of Petroleum Engineering, Beijing Key Laboratory of Urban Oil and Gas Distribution Technology, China University of Petroleum-Beijing, Fuxue Road No. 18, Changping District, Beijing, 102249, PR China
[c] CNOOC Research Institute Co. Ltd, Beijing, 100028, PR China
[d] PipeChina North Pipeline Company, LangFang, 065000, PR China
[e] College of Chemical Engineering, Fuzhou University, Fuzhou, 350108, PR China

ARTICLE INFO

Article history:
Received 10 November 2021
Received in revised form
11 January 2022
Accepted 11 January 2022
Available online 19 January 2022

Edited by Xiu-Qiu Peng

Keywords:
Gas-solid flow
Erosion
304 stainless
L245 carbon steel
Erosion model

ABSTRACT

Erosion is one of the most concerning issues in pipeline flow assurance for the Oil & Gas pipeline industries, which can easily lead to wall thinning, perforation leakage, and other crucial safety risks to the steady operation of pipelines. In this research, a novel experimental device is designed to investigate the erosion characteristics of 304 stainless and L245 carbon steel in the gas-solid two-phase flow. Regarding the impacts on erosion rate, the typical factors such as gas velocity, impact angle, erosion time, particle material and target material are individually observed and comprehensive analyzed with the assistance of apparent morphology characterized via Scanning Electron Microscope. Experimental results show that the severest erosion occurs when the angle reaches approximate 30° whether eroded by type I or type II particles, which is observed in both two types of steel. Concretely, 304 stainless steel and L245 carbon steel appear to be cut at low angles, and impacted at high angles to form erosion pits. In the steady operational state, the erosion rate is insensitive to the short erosion time and free from the influences caused by the "erosion latent period". Based on the comparison between experimental data and numerical results generated by existing erosion models, a modified model with low tolerance (<3%), high feasibility and strong consistency is proposed to make an accurate prediction of the erosion in terms of two types of steel under various industrial conditions.

1. Introduction

Technological advances in hydraulic fracturing and horizontal drilling have driven the worldwide exploitation of shale gas (Hong et al., 2020). However, a large amount of particle will be carried in the process of shale gas exploitation (Hong et al., 2021a). During the flow of gas carrying particle in the pipeline, solid particles continuously impact the inner surface of the pipeline (Wang et al., 2021), and the material will gradually be removed from the inner wall of the pipeline and equipment (Jia et al., 2021). The erosion can easily lead to wall thinning, perforation leakage and other problems, and cause significant safety risks to the safe operation of pipelines (Hong et al., 2021b; Peng et al., 2021).

In recent years, the erosion problem in the oil and gas industry has attracted extensive attention of researchers, and three methods are employed to investigate erosion, including theoretical analysis (Parsi et al., 2014), numerical simulation (Abduljabbar et al., 2021) and experimental research (Wang et al., 2021). In theoretical analysis methods, the Lagrange approach is used to predict the particle trajectory, and then the first and second collision velocities are calculated (Kang and Liu, 2020). Using the trajectory probability of a single particle, the probabilistic behavior of a large number of particles in the bend is derived, and the erosion distribution caused by the first and second collisions in the bend can be calculated (Kang and Liu, 2020; Wang et al., 2017). As for the numerical simulation of erosion, it is mainly based on Computational Fluid Dynamics software to model the fluid flow process, turbulence

* Corresponding author.
** Corresponding author.
E-mail addresses: xpli126@126.com (X. Li), ydgj@cup.edu.cn (J. Gong).

https://doi.org/10.1016/j.petsci.2022.01.011

models are used for fluid and particle flow simulation (Bilal et al., 2021), and empirical erosion models are used for erosion calculation (Abduljabbar et al., 2021; Alghurabi et al., 2021). Finally, the results of particle concentration, particle flow rate, wall collision velocity, wall erosion amount and so on can be obtained (Tang et al., 2021).

Many researchers have conducted erosion experiments to obtain more direct and intuitive results. The measurement of gas velocity and particle velocity is mainly through the particle image velocimetry (PIV), which uses the tracer particles in the flow field without interfering with the flow field (Novelletto Ricardo and Sommerfeld, 2020; Wang et al., 2019). A. Mansouri et al. (2015) employed PIV to determine the slip velocity between gas and particle in horizontal and inclined pipes, and measured the local erosion depth with contour scanner to study the effects of erosion angle and gas velocity on erosion results. By comparing PIV and PTV, Lin et al. (2018) concluded that the PIV device has a relatively reliable calculation accuracy when measuring the flow field with high velocity and small particle size (Lin et al., 2015). The erosion degree is mainly evaluated by weight loss and wall thickness loss. However, Solnordal et al. (2015) believed that it difficult to obtain specific erosion conditions at specific locations by using weight loss evaluation. Therefore, they used a surface profilometer to record surface loss conditions of target materials. The experimental results showed that the maximum erosion location occurs between 55° and 60° of the elbows, and the depth of erosion decreases uniformly in all directions from this point. The three-dimensional scanner is used to accurately measure the erosion wall thickness changes of vulnerable parts such as elbows and ball valves (Zhang et al., 2015; Zheng et al., 2019). Wong et al. (2013) designed an experimental device to explore the erosion law of the cavity, and used the inner coating technology to qualitatively observe the erosion under the impact of sand and gravel. Vieira et al. (2016) used ultrasonic technology to measure the erosion at different points by marking 16 different points on the outside of the elbow.

The influencing factors of erosion mainly include gas velocity (Islam and Farhat, 2014), particle size (Nguyen et al., 2016), material and shape of particles (Arabnejad et al., 2015; Xie et al., 2021), the impact angle (Nandre and Desale, 2018; Nguyen et al., 2014) and so on (Javaheri et al., 2018). Oka and Yoshida (2005) believed that the degree of erosion damage is not only related to the flow field and the properties of particles, but also related to the target material (Oka et al., 2009). The erosion law is studied by the impact of SiC, SiO_2 and glass beads materials on aluminum, copper, carbon steel and stainless steel (Oka et al., 2005). Meanwhile, the experiments also investigated the degree of damage caused by the angle of impact on different materials, and the conclusion showed that the hardness of target material is an indispensable factor. Finally, a general erosion prediction equation which can be used in any impact condition and any type of material was proposed (Oka et al., 2005). Liu et al. (2015) showed that the erosion rate could be effectively reduced by increasing the bending radius of the elbow. When actual operating space is limited, a tee can be used instead of an elbow to reduce the erosion rate. Recently, Wang et al. (2021) performed an experimental and numerical study of slurry erosion behavior in a horizontal elbow and elbows in series. It was found that the maximum erosion location changes to the extrados of the elbow when velocity increases. The above researches have promoted the understanding and quantitative calculation of the gas-solid two-phase erosion law. However, the composition of particle in the study area is complex, and its erosion has not been explored in the existing model and experimental research. A vital knowledge gap exists in understanding the erosion between particles and pipelines of different materials in the gas field.

In this work, the self-designed experimental device is employed to investigate gas-solid two-phase erosion according to the on-site working conditions, including the on-site particle, 304 stainless steel and L245 carbon steel. The effects of gas velocity, impact angle, erosion time and target material on the erosion rate are explored, and the apparent morphology is observed by Scanning Electron Microscope (SEM). By comparing the erosion experimental results with the existing erosion models, a modified model for different specimen materials is proposed to improve the accuracy of the model for meeting the engineering practical application standards.

The structure of this paper is as follows. In section 2, the materials and methods is explained in detail, including the apparatus and materials, experimental procedures and the definition of erosion speed and erosion rate. section 3 presents the results of the impact of typical factors on erosion rate, such as gas velocity, impact angle, erosion time, particle material and target material. Finally, the conclusion and future research prospects are drawn in section 4.

2. Materials and methods

2.1. Apparatus and materials

The experiment was carried out on a gas-solid two-phase erosion device, as shown in Fig. 1. The device consists of four parts: compression system, feeding system, erosion system and particle recovery system. The air enters the pipe after being compressed by the twin-screw air compressor, and the flow rate of air is controlled by adjusting the opening of the ball valve. Then, the gas passes through the feeding system, mixes with solid particles, accelerates together, and then is ejected from the nozzle to erode the test specimen. Finally, the eroded particles are collected by the cyclone separator. The whole device is built of 1 inch pipe with inner diameter of 25 mm.

The compression system (Fig. 2a) mainly includes two twin-screw air compressors (SA22A), buffer tanks, ball valves, flow meters (MF5712), etc. The maximum supply pressure is 0.85 MPa, and the air flow rate is 3.4 Nm^3/min. The twin-screw air compressors are capable of supplying air continuously with tiny pressure fluctuation. They can run empty after the pressure reaches the maximum set value, and start automatically when the pressure drops below the minimum value. The gas is compressed into five gas buffer tanks that can withstand a pressure of 1 MPa, which can reduce the pressure fluctuation and store the air to ensure that the erosion device is supplied with sufficient and stable airflow.

The feeding system (Fig. 2b) consists of feeding funnels, screws, motors and other structures. Particles are transported to the feeding port by the screw rod at the bottom of the feeding funnel. The speed of the motor can be controlled by changing the frequency of the motor, thereby changing the rotation speed of the screw. The higher the frequency, the faster the rotation speed and particle feeding speed, and the greater the mass flow rate of the particles. Moreover, the air flows in the pipe at low pressure, and the particles in the hopper are pushed into the pipe from the feed port through the hose under the action of the pressure differential to mix with the air.

The erosion system (Fig. 2c), housed in a plexiglass container, consists of a nozzle, an eroded specimen, a specimen base, a glass cover, etc. The nozzle outlet diameter is 8 mm, a metal cylindrical specimen with a diameter of 30 mm and a thickness of 3 mm is fixed on a base in the erosion system. The impact angle of particles can be changed by adjusting the installation angle of the specimens between 0° and 90°. In addition, the glass cover outside the erosion system can effectively prevent particles from diffusing into the laboratory and polluting the environment of the lab.

The particle recovery system (Fig. 2d) consists of two cyclone separators, a blower, and hoses. The two-stage cyclone separation

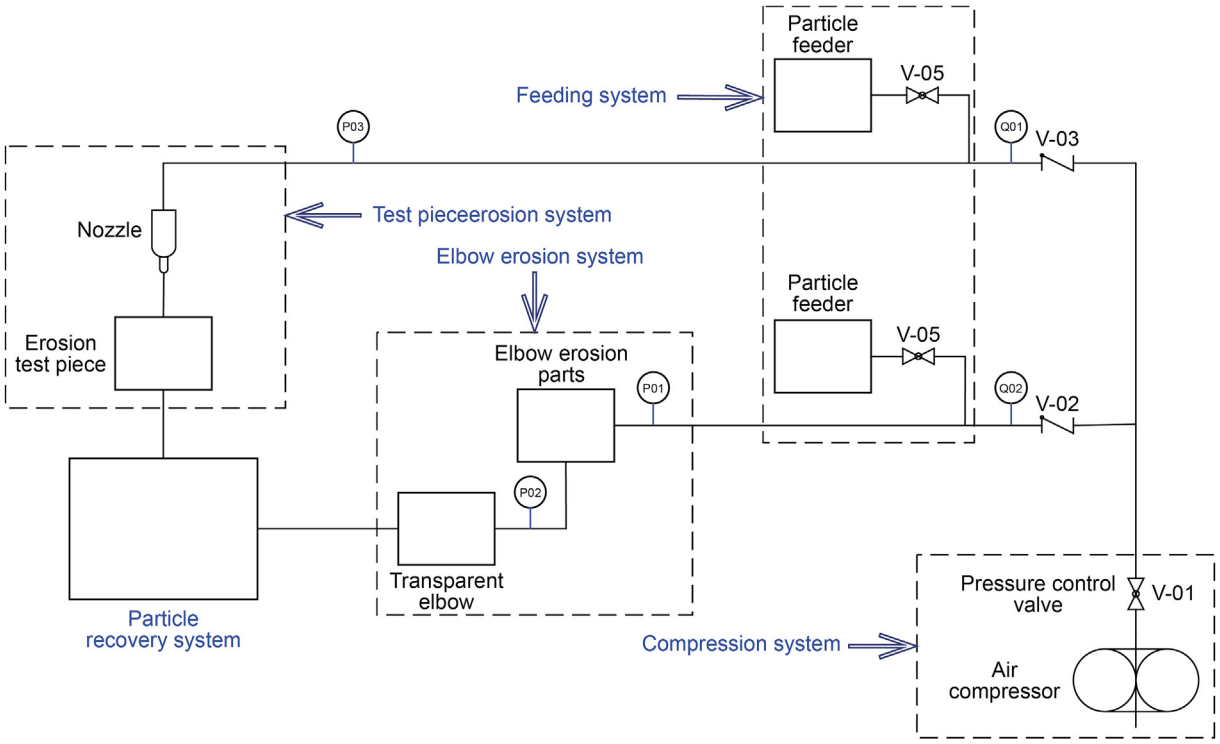

Fig. 1. Schematic diagram of the gas-solid two-phase erosion device.

can store and recover the particles used in the experiment more efficiently, which saves the experimental cost and avoids polluting the laboratory environment. Before the experiment, the blower is turned on to suck air into the device, and particles enters the cyclone separator under the action of pressure differential.

304 stainless steel and L245 carbon steel are selected based on the usage on site. 304 stainless steel is a common material in stainless steel, containing more than 18% of chromium and more than 8% of nickel. It can withstand high temperature of 800 °C, and has the characteristics of good processability, high toughness and corrosion resistance. Therefore, it is widely used in pipelines that require corrosion protection in the shale gas development industry. As for L245 carbon steel, it is mainly used to make seamless steel pipes for the transportation of natural gas and oil. The significant difference between the two is that 304 stainless steel contains chromium and nickel. The specific chemical composition is shown in Table 1.

The specimens of 304 stainless steel and L245 carbon steel with the diameter of 30 mm were polished smooth with sandpaper before each experiment to avoid experimental errors caused by different surface roughness. A high-precision balance made by Metter Toledo, model XS205 with the accuracy of 0.1×10^{-3} g was used to evaluate erosion through weight loss.

Two types of particles were used in the experiment, type I particle and type II particle. Type I particle consists of 60 mesh (150 μm) quartz sand whose SEM picture is shown in Fig. 3a. Type II particle from the production site is composed of 70% pottery and 30% quartz sand. The pottery is mainly spherical and with a size between 40 mesh and 70 mesh, while the particle size of type II particle is mainly between 70 mesh and 140 mesh. It was observed that the type II particle is irregular ellipsoid with convex surface.

2.2. Experimental procedures

The weighing method was used to evaluate the degree of erosion. In order to ensure the stability of the experimental results, each group of experiments was repeated three times under the same conditions, and the effective experimental results were selected and the average value was calculated.

Step 1 Before the start of the experiment, use sandpaper to polish the surface of the specimen smoothly, clean the surface of the metal chips, weigh the specimen and clamp it on the base.

Step 2 Set gas velocity as predetermined, and then adjust the motor frequency of the feeding system to make the particle enter the pipe as the set mass flow rate, mix with the gas, thereby corroding the specimen. Each group of experiments consumes a certain quality of particles, then the gas and power supply of the compressor is cut off to end the experiment.

Step 3 Take off and weigh the specimen, then calculate the erosion rate of this group of experiments. The erosion speed E and the erosion rate ER are used as criteria for measuring the erosion loss of the specimen. Erosion speed E is the ratio of mass loss to the time, while erosion rate ER is the ratio of mass loss to the mass of particles (Arabnejad et al., 2015), which are defined as follows.

$$E = \frac{m_s}{t} = \frac{m_{s1} - m_{s2}}{t} \tag{1}$$

$$ER = \frac{m_s}{m_p} = \frac{m_{s1} - m_{s2}}{m_p} \tag{2}$$

where m_{s1} is the mass of the specimen before the experiment, m_{s2} is the mass of the specimen after the experiment, t is the total time of each group of experiments, and m_p is the total mass of the particle used in each group of experiments.

It can be seen from the definition formula that the erosion speed E characterizes the speed of erosion and is related to time; the erosion rate ER characterizes the severity of erosion and is related to the quality of the particles.

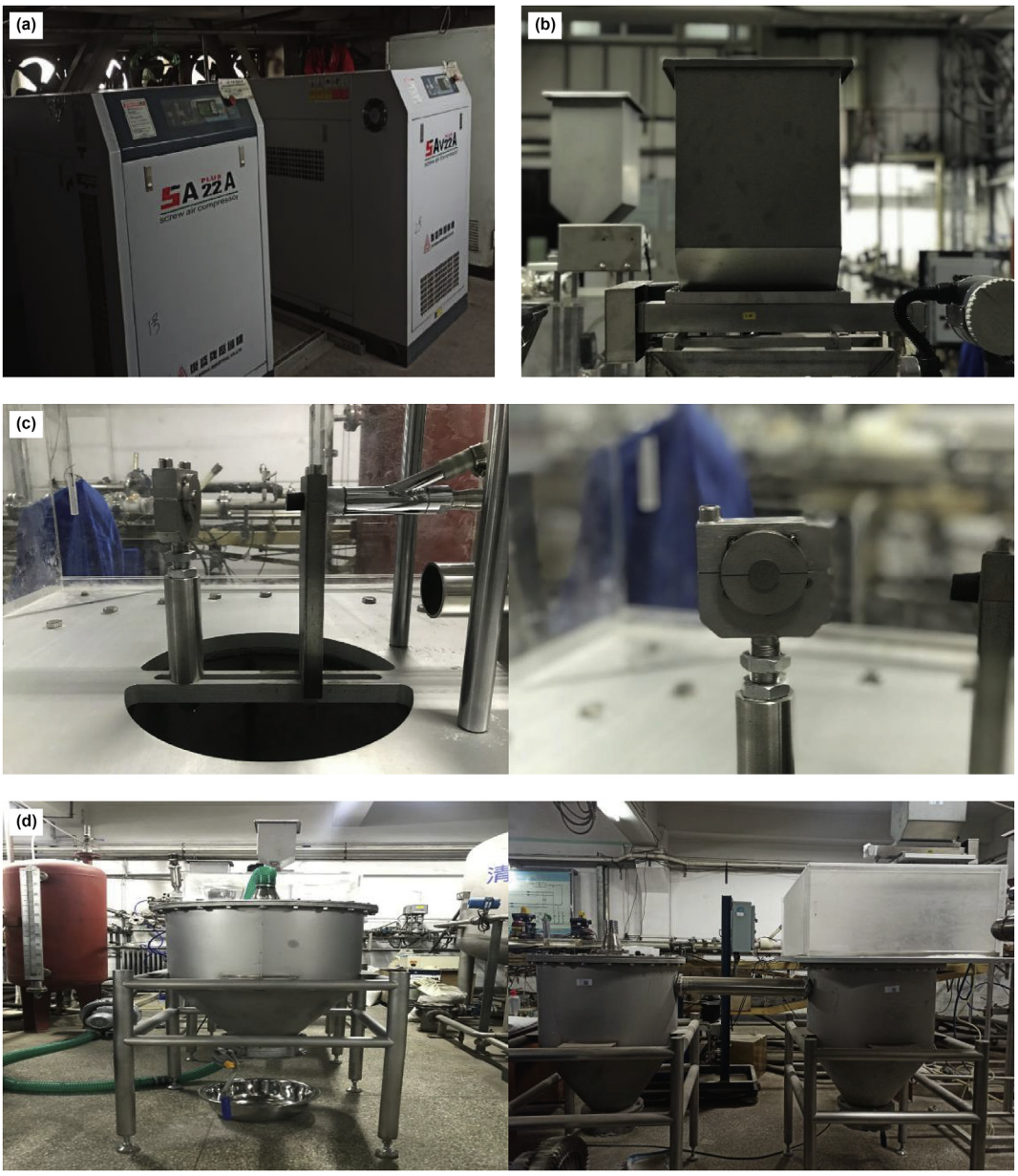

Fig. 2. Gas-solid two-phase erosion device: (a) compression system, (b) feeding system, (c) erosion system and (d) particle recovery system.

Table 1
Chemical compositions of 304 stainless steel and L245 carbon steel (%).

	Mo	Mn	Ni	Cr	Si	Cu	C	S	N
304 stainless steel	0.01	0.27	8.23	18.16	0.24	0.31	0.051	0.004	0.033
L245 carbon steel	0.055	1.08	0.013	0.024	0.20	-	0.069	0.0026	-

Step 4 Wash the oil and sand off the specimen surface with acetone, and then observe the changes of specimen surface with SEM to explore the erosion mechanism.

3. Results and discussion

3.1. Effect of particle mass flow rate on E & ER

The 304 stainless steel was selected and the erosion angle was set to 90°. 50 kg of type I particle was used in each group of experiments, which was mixed uniformly with gas in the pipe through the feeding system. The gas flow rate was measured by the flowmeter in front of the nozzle, and the rotational speed of the motor of the feeding system was adjusted to change the grit mass flow rate. The results shown in Fig. 4a indicates that, (a) In the case of fixed conditions such as erosion speed, angle and particle quality, the erosion speed *E* of 304 stainless steel increases uniformly with the increase of the particle mass flow rate. For example, when the gas flow rate is 26.62 m/s, the erosion speed *E* changes from 0.012 mg/s to 0.025 mg/s as the mass flow rate changes from 4.79 g/s to 11.11 g/s. (b) When other conditions are fixed, the greater the gas velocity in the pipe, the greater the erosion speed *E*. In addition,

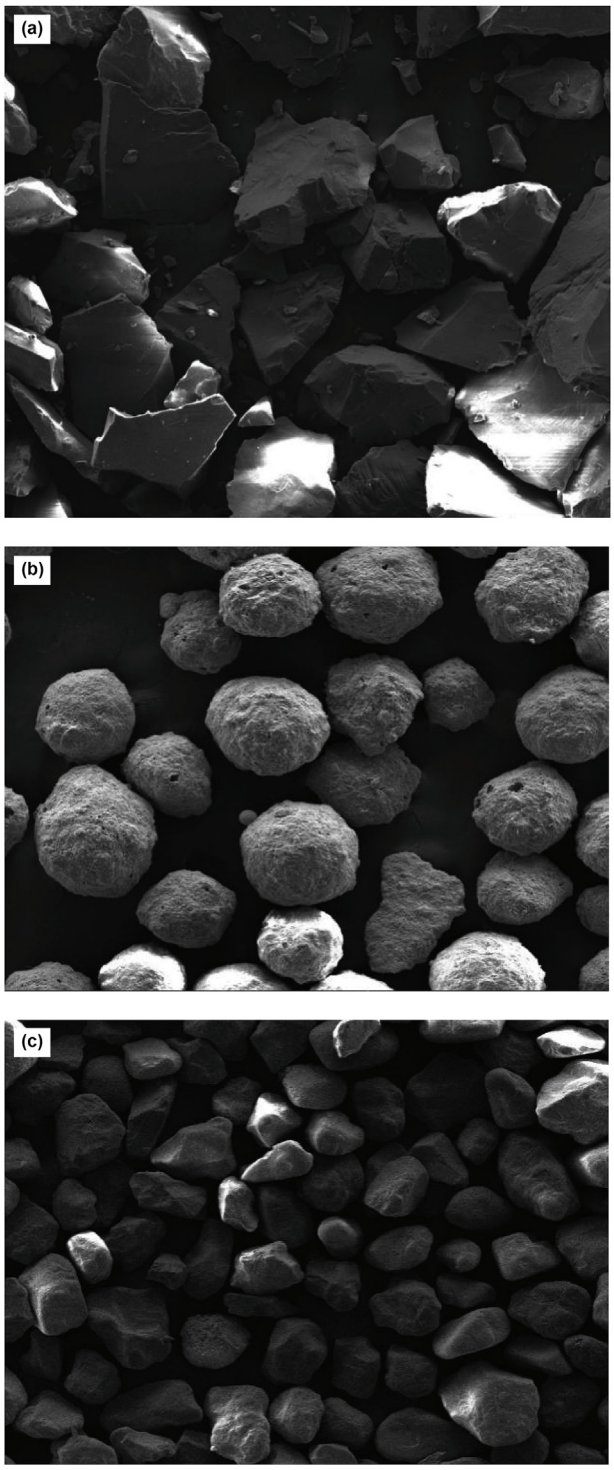

Fig. 3. Experimental particle: (a) type I particle, (b) pottery of type II particle and (c) quartz sand of type II particle.

the greater the gas velocity, the greater the erosion speed E changes with the particle mass flow rate, indicating that the erosion speed E with the particle mass flow rate are more sensitive to large gas velocity.

Taking the ratio of the erosion mass to the particle mass flow rate in Fig. 4a, the correlation between the erosion rate and the particle mass flow rate can be obtained, as shown in Fig. 4b. Under the specified gas velocity, the particle mass flow rate has little effect on *ER*, and even weakens the effect. That is, *ER* decreases with the increase of particle mass flow rate when other conditions are fixed. In other words, when other factors are fixed, with the particle mass flow rate increasing, the mass loss of the target material is roughly the same as long as the total mass of particle is fixed.

The main reasons for this phenomenon are the following three processes. First, when the gas velocity increases, the particles in the pipe have greater velocity under the carrying of gas, and according to the momentum theorem, the greater stress is generated when the particles impact the target surface. Therefore, when the gas velocity is large, the *ER* is greater. Second, with the increase of the particle mass flow rate, the particle on the cross-sectional area of the pipe will also increase, which will aggravate the collision of particle and consume the kinetic energy of particle. Therefore, the *ER* begins to decrease with the mass flow rate. Last, at a certain gas velocity, the particle -carrying capacity of the gas in the pipe is limited. When the mass of particle gradually increases, the particle cannot reach the gas velocity or cannot be blown up. Hence, the particle accumulates at the bottom of the pipe. As a result, the *ER* cannot increase with the particle mass flow rate gradually, but even decreases.

3.2. Effect of gas velocity on ER

The 304 stainless steel was selected and the erosion angle was set to 90°. 50 kg of type I particle was used in each group of experiments. The particle mass flow rates were 10 g/s and 12 g/s, and the gas velocities were 26.20 m/s, 28.82 m/s, 31.43 m/s and 36.67 m/s. The relationship between *ER* and gas velocity of 304 stainless steel under impact angle 90° is shown in Fig. 5. With the increase of gas velocity, the *ER* increases gradually. For example, when the gas velocity is 26.62 m/s, the *ER* is about 2.3 mg/kg. When the gas velocity gradually increases to 28.82 m/s, 31.43 m/s and 36.67 m/s, the *ER* of the target material gradually increases from 2.8 mg/kg to 5.8 mg/kg. In addition, the difference between *ER* at mass flow rate of 12 g/s and that at mass flow rate of 10 g/s are minimal, which is also consistent with Section 3.1 that *ER* shows little relationship with particle mass flow rate.

The L245 carbon steel was selected and the erosion angle was set to 90°. 50 kg of type II particle was used in each group of experiments and the particle mass flow rates were 10 g/s. The experiments were conducted under the gas velocity of 20.96 m/s, 26.20 m/s, 31.43 m/s, 34.03 m/s, 36.68 m/s and 41.92 m/s. As shown in Fig. 6, similar to the 304 stainless steels, the *ER* of L245 carbon steel has the same change law with the change of gas velocity.

Extensive literature shows that there is an exponential relationship between erosion rate *ER* and gas velocity v:

$$ER = K_m v^n \tag{3}$$

Where K_m is a constant coefficient, n is the speed index and is related to the type of the material.

The power function is used to regress the curve in Figs. 5 and 6, and Eq. (4) and Eq. (5) can be obtained, respectively:

$$ER = 0.000003 v^{2.789} \tag{4}$$

$$ER = 0.0001 v^{2.9316} \tag{5}$$

For different types of materials, the value range of n is different. For plastic materials, the velocity index n is generally between 2 and 3. For brittle materials, the velocity index n is generally between 4 and 6. 304 stainless steel is plastic material, and the value of n in Eq. (4) is 2.789, which is consistent with the results obtained by Oka et al. (2005), Oka and Yoshida (2005).

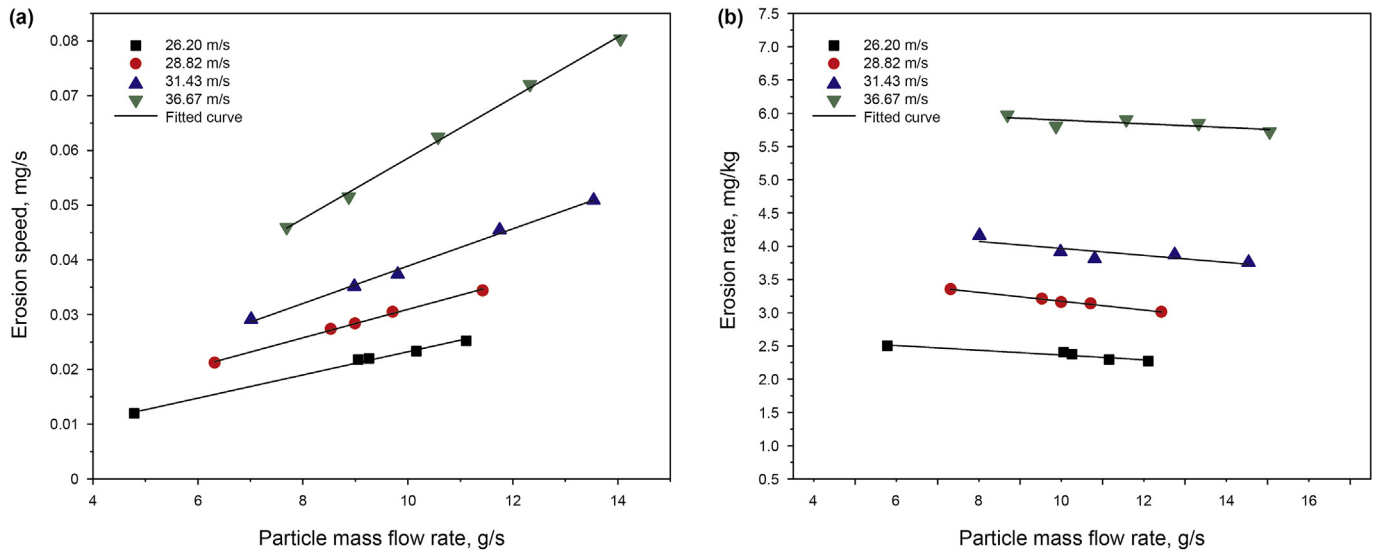

Fig. 4. Effect of particle mass flow rate on *E*& *ER* under different gas velocity.

3.3. *Effect of impact angle on ER*

For each group of experiments, 50 kg particle was used. The effect of the erosion angle on the *ER* was investigated at 15° intervals between 0° and 90°, and the microscopic surface morphology of the target material was observed at each erosion angle. Then, the *ER* at each erosion angle was normalized, i.e., the erosion rate at each erosion angle was divided by the erosion rate at the erosion angle of 90°.

As shown in Fig. 7, the *ERs* of 304 stainless steel and L245 carbon steel have the same change law under different impact angles. The *ER* of both materials reach the maximum at about 30° under the impacts of type I or type II particle. When the impact angle is less than 30°, the *ER* increases as the impact angle increases, while when the impact angle is greater than 30°, the *ER* decreases as the impact angle increases. In addition, under the same conditions, the *ER* caused by type I particle is higher than that by type II particle. By comparing the erosion morphology of the two types of particles at the same erosion angle, it can be found that the shape of type I is sharper, and the groove and the contour of erosion pit formed by type I are more obvious than type II, so the *ER* caused by type I is also larger.

304 stainless steel and L245 carbon steel are ductile materials. According to Finnie's erosion theory (Finnie, 1960), the erosion of ductile materials is mainly based on cutting at low angles. The wall surface morphology of 304 stainless steel and L245 carbon steel was observed by the SEM. The results show that 304 stainless steel and L245 carbon steel appear to be cut at low angles, and to be impacted at high angles to form erosion pits. As shown in Fig. 8a and Fig. 8b, when the particle washes the surface of the target material at the angle of 30°, the particle will cut the surface like a sharp knife. At the same time, grooves and lip edges will be formed on the surface washed away by the particle. According to Bitter's erosion theory (Bitter, 1963a, 1963b), when the particle impacts the surface at 90°, the speed of the particles hitting the surface of the material is fast, so the stress generated by the impact on the wall is

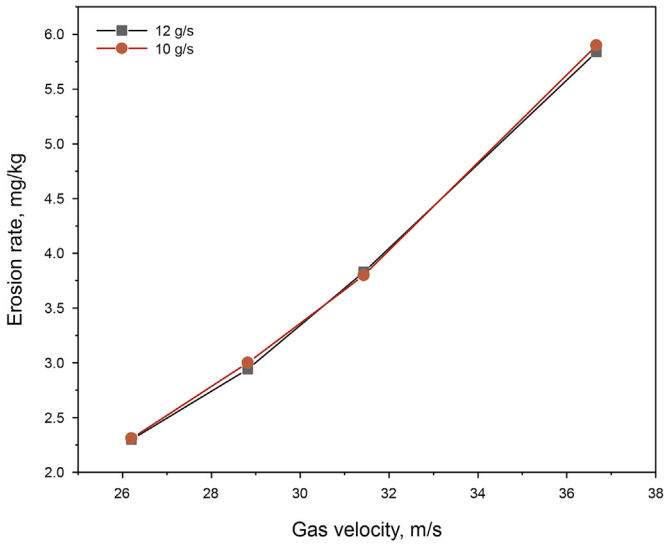

Fig. 5. Effect of gas velocity on *ER* of 304 stainless steel.

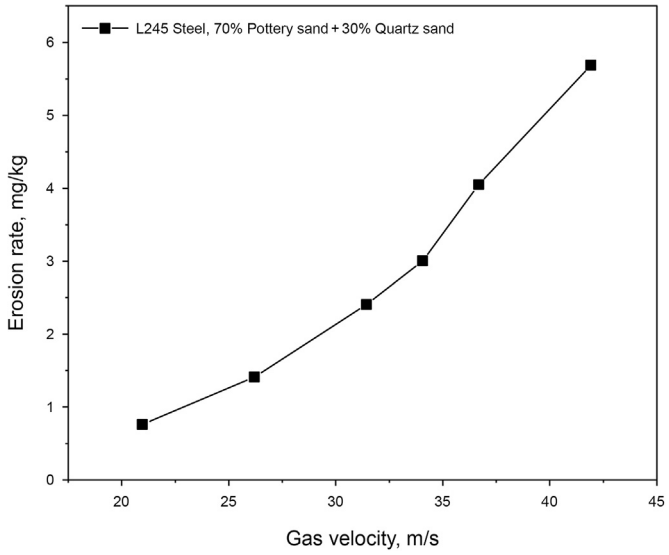

Fig. 6. Effect of gas velocity on *ER* of L245 carbon steel.

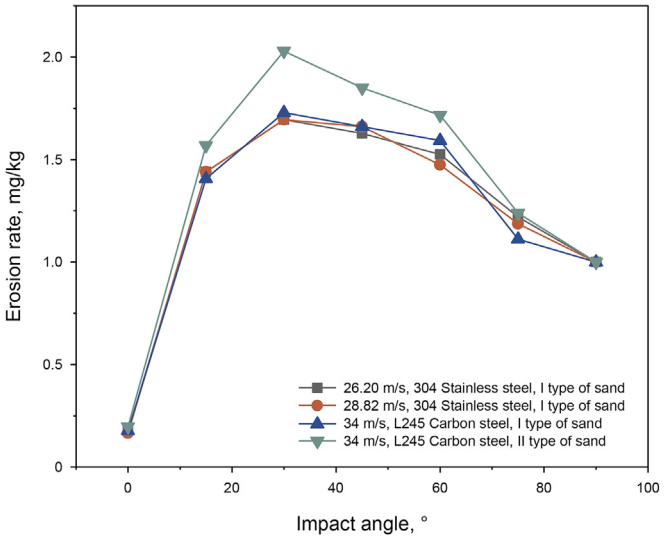

Fig. 7. Effect of impact angle on *ER*.

greater than the yield strength of 304 stainless steel. Therefore, as shown in Fig. 8 (c) (d), the materials will gradually fall off the surface of the target material and erosion pits are formed.

The surface morphology of L245 carbon steel eroded by type I and II particle at different angles is provided in Appendix. Under low angles of erosion (impact angles less than 30°), grooves will be formed on the target material surface in the shape of strips cut by particles, meanwhile a lip is extruded around the grooves. When the impact angle gradually increases (impact angles greater than 30°), the grooves and lips edges gradually disappear and are replaced by erosion pits.

3.4. Effect of erosion time on ER

Set a specified sand mass flow rate, and the erosion time can be judged by the particle weight used in erosion experiment. The heavier the mass of particle used, the longer the erosion time. The experimental results of 304 and L245 carbon steel specimen are shown in Fig. 9. The longer the erosion time, the greater the quality loss of the specimen and the more serious the erosion. However, the erosion rate is a relative ratio, which is the ratio of mass loss to the mass of eroded particles. It is found through experiments that

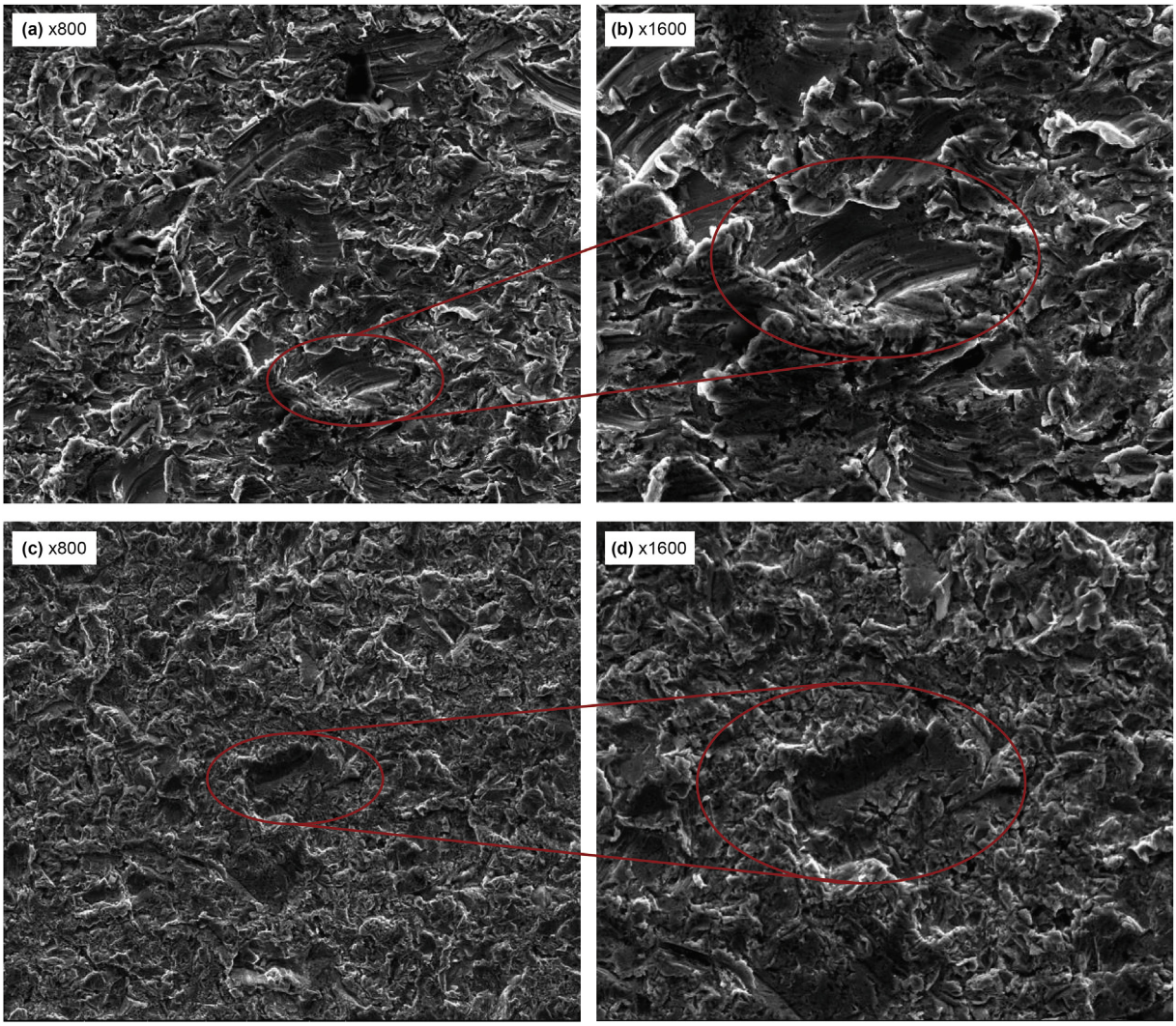

Fig. 8. Surface morphology of 304 stainless steel, (a) (b) impact angle of 30°, (c) (d) impact angle of 90°.

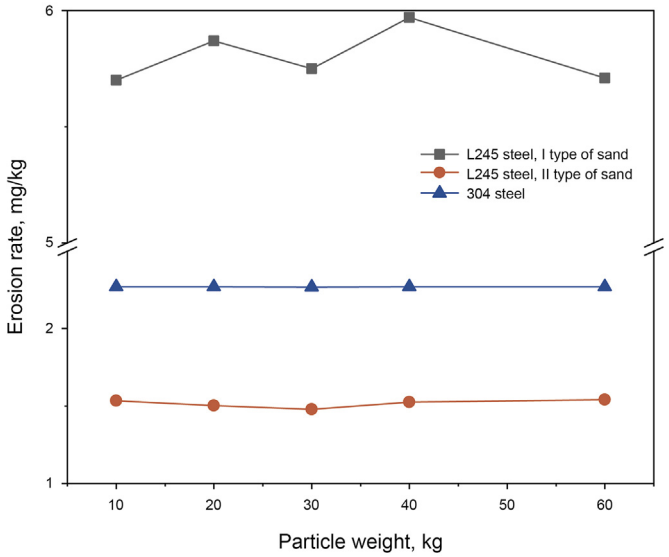

Fig. 9. Effect of erosion time on *ER*.

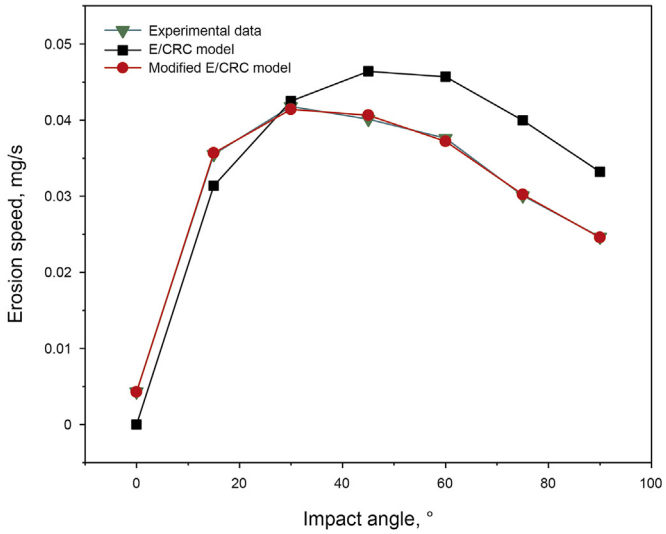

Fig. 11. Comparison between experimental data and calculated results.

the erosion time has no significant effect on the erosion rate. Previous studies have shown that the *ER* will gradually increase from 0 and then gradually rise with the increase of sand weight, until it finally reaches a state where *ER* tends to be stable. The former stage is called the erosion latent period, and the latter stage is called the erosion stable period. When a small amount of particle erodes the surface of the ductile material specimen, some of the material on the specimen surface does not fall off immediately, but forms a lip around the groove. A specified gas velocity, the particle -carrying capacity of the gas in the pipe is limited. Therefore, the *ER* in the initial stage of erosion, i.e., erosion latent period is low. As the particle keeps hitting the surface of the specimen, the lip comes off and the erosion reaches a stable stage. Since the time of "erosion latent period" is very short for this experiment and the actual field operation, the *ER* is not affected by the erosion time when the erosion conditions remain stable.

3.5. Modification of erosion model

Three conventional erosion models E/CRC model (Zhang et al., 2007), Ahlert model (Ahlert, 1994), DNV model (Peng and Cao, 2016; Song et al., 2013; Veritas, 2007) were conducted under experimental conditions, the mass flow rate of 0.01 kg/s, gas velocity of 26.62 m/s, erosion angle of 90°, and 304 stainless steel specimens. The comparison between experimental data and calculated results are shown in Fig. 10. The maximum impact angle is between 40° and 50°, 55°–65° and 25°–35° obtained by the E/CRC model, DNV model and Ahlert model, respectively. The predicted accuracy of DNV model is the lowest among the three models. There is a large deviation between the predicted value and the experimental data under various conditions, where the maximum relative error reaches 61.18%. Therefore, it's obvious that the DNV model cannot meet the prediction criteria. In addition, the average relative tolerance rates of E/CRC model and Ahlert model are 19.68% and 22.41%, respectively. The above three models fail to meet the industrial criteria. Hence, the E/CRC model with the

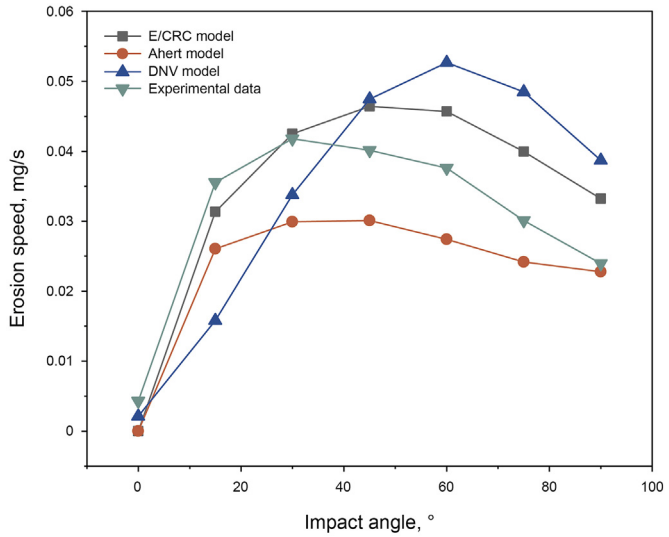

Fig. 10. Comparison between experimental data and calculated results.

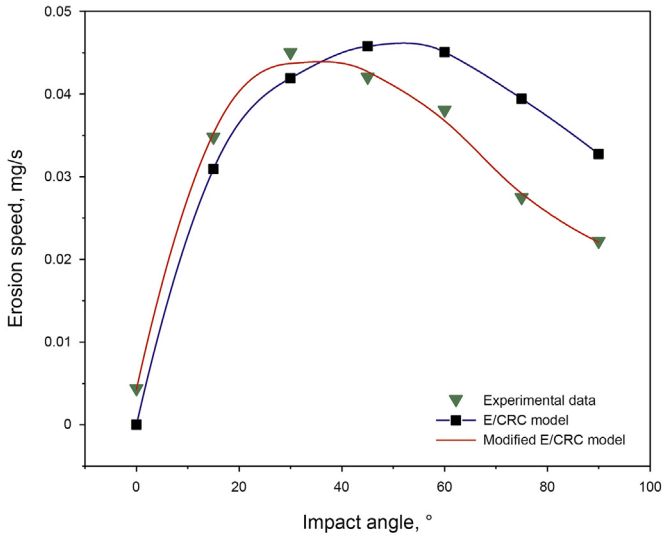

Fig. 12. Comparison between experimental data and calculated results.

smallest relative tolerance was selected for modification.

The E/CRC model is modified based on the experimental data of 304 stainless steel as follows:

$$ER = 0.6639 \cdot BH^{-0.59} \cdot F_s \cdot v_p^{2.783} \cdot f(\alpha) \tag{6}$$

where BH is Brinell hardness, F_s is gravel shape factor, v_p is particle impact velocity, α is particle impact angle, and

$$f(\alpha) = 2.91\alpha^5 - 13.15\alpha^4 + 22.90\alpha^3 - 20.06\alpha^2 + 8.77\alpha + 0.17 \tag{7}$$

The calculated results of modified E/CRC model are shown in Fig. 11. The maximum relative tolerance is 1.78% under this working condition, which is much smaller than that of the original E/CRC model. The simulation results of the modified E/CRC model have smaller tolerances and can make accurate prediction of the erosion results under this experimental condition.

Similarly, the E/CRC model is modified based on the experimental data of L245 carbon steel as follows:

$$ER = 0.4087 \cdot BH^{-0.59} \cdot F_s \cdot v_p^{2.897} \cdot f(\alpha) \tag{8}$$

where

$$f(\alpha) = 1.87\alpha^5 - 8.32\alpha^4 + 15.35\alpha^3 - 15.98\alpha^2 + 8.61\alpha + 0.19 \tag{9}$$

The calculated results of E/CRC model after modification are shown in Fig. 12. The maximum relative error is 3.95% at this experimental condition. The relative error in this set of experimental conditions is much smaller than that of the original E/CRC model. The simulation results of the modified E/CRC model have smaller errors and can make accurate prediction of the erosion results under this experimental condition.

4. Conclusions

(1) A gas-solid two-phase erosion device is designed and manufactured, which consists of air supply system, feeding system, erosion system and particle recovery system. The device can flexibly control the gas flow rate and particle mass rate, and it is convenient to alternate the specimen and adjust the angle.

(2) Due to the smaller hardness of L245 carbon steel, the erosion of L245 carbon steel is severer than that of 304 stainless steels under the same conditions. With the particle mass flow rate increasing, as long as the total mass of particle is fixed, the mass loss of the target material is roughly the same. The *ER* of both materials reach the maximum at about 30° under the impacts of type I or type II particle. 304 stainless steel and L245 carbon steel appear to be cut at low angles, and to be impacted at high angles to form erosion pits. In particular, under low angles of erosion (impact angles less than 30°), grooves will be formed on the target material surface in the shape of strips cut by particle, meanwhile a lip is extruded around the grooves. When the impact angle gradually increases (impact angles greater than 30°), the grooves and lips edges gradually disappear and are replaced by erosion pits. Since the time of "erosion latent period" is very short for this experiment and the actual field operation, the *ER* is not affected by the erosion time in the steady operational state.

(3) By comparing the calculation results of the E/CRC model, Ahlert model and DNV model to the experimental data, the tolerance of each model is large and cannot meet the industry criteria. Therefore, the modified E/CRC model is proposed for 304 stainless steel and L245 carbon steel, respectively. The average relative error of the modified models for the two target materials is within 3%, which can make accurate prediction of the erosion results and meet the industrial requirements.

(4) Shale gas in gathering and transmission pipelines usually contains small solid particles and acid liquids such as dissolved CO_2. Therefore, the coexistence of solid particle erosion and acid corrosion is a common phenomenon in shale gas gathering and transmission pipeline. In the future, we will further transform the experimental device to study the synergistic mechanism of erosion and corrosion. Nevertheless, our findings provide a theoretical support for the erosion of two-phase gas-solid flow in 304 stainless/L245 carbon steel to solve the flow assurance issue in the oil & gas pipelines.

Declaration of competing interest

The authors declare that they have no known competing financial interests or personal relationships that could have appeared to influence the work reported in this paper.

Acknowledgements

This work was supported by the Zhejiang Province Key Research and Development Plan (2021C03152), Zhoushan Science and Technology Project (2021C21011), Industrial Project of Public Technology Research of Zhejiang Province Science and Technology Department (LGG18E040001), and Scientific Research Project of Zhejiang Province Education Department (Y20173854), all of which are gratefully acknowledged. Thanks to Zhouyin He and Yulin Liu for English language editing.

Appendix

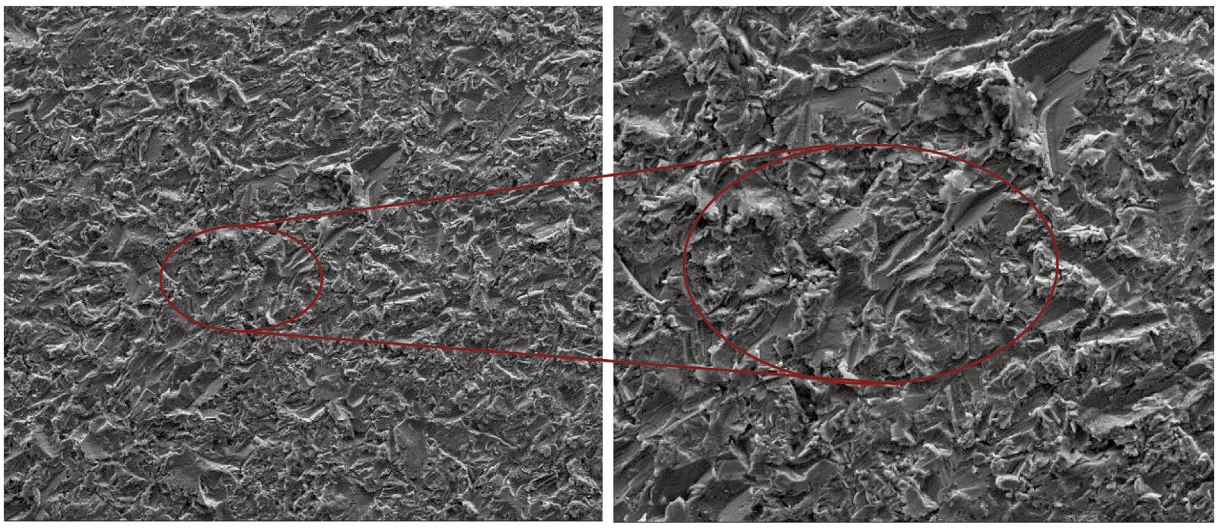

Fig. A1. Surface morphology of L245 carbon steel at 15° (type I particle).

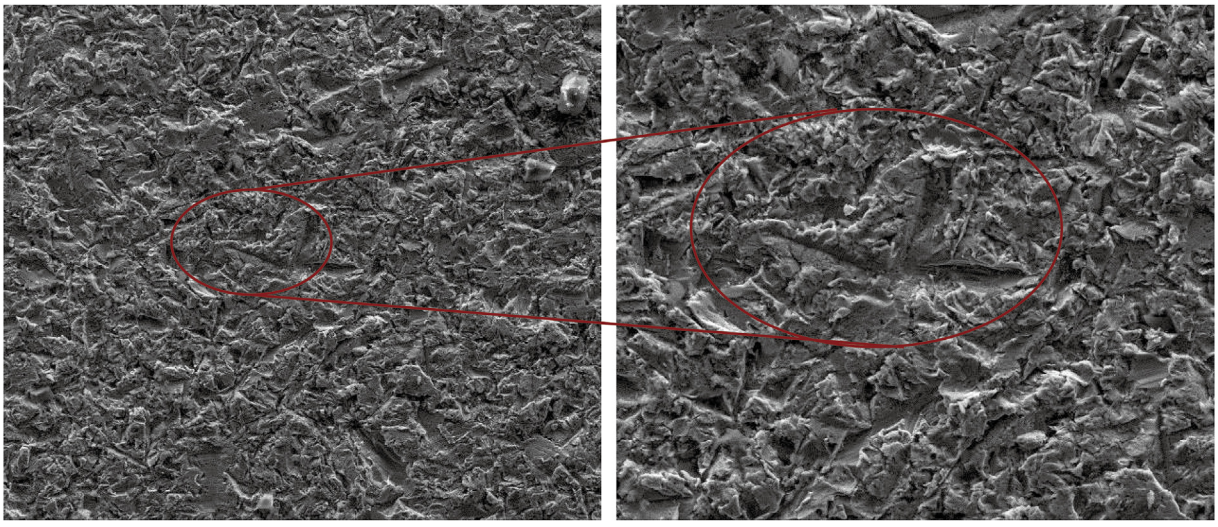

Fig. A2. Surface morphology of L245 carbon steel at 30° (type I particle).

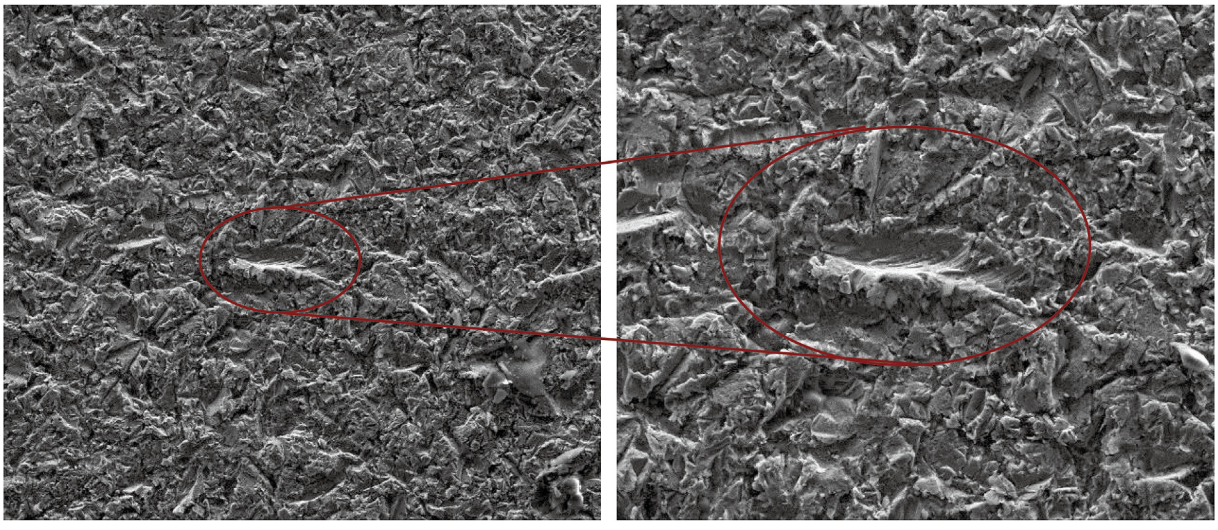

Fig. A3. Surface morphology of L245 carbon steel at 45° (type I particle).

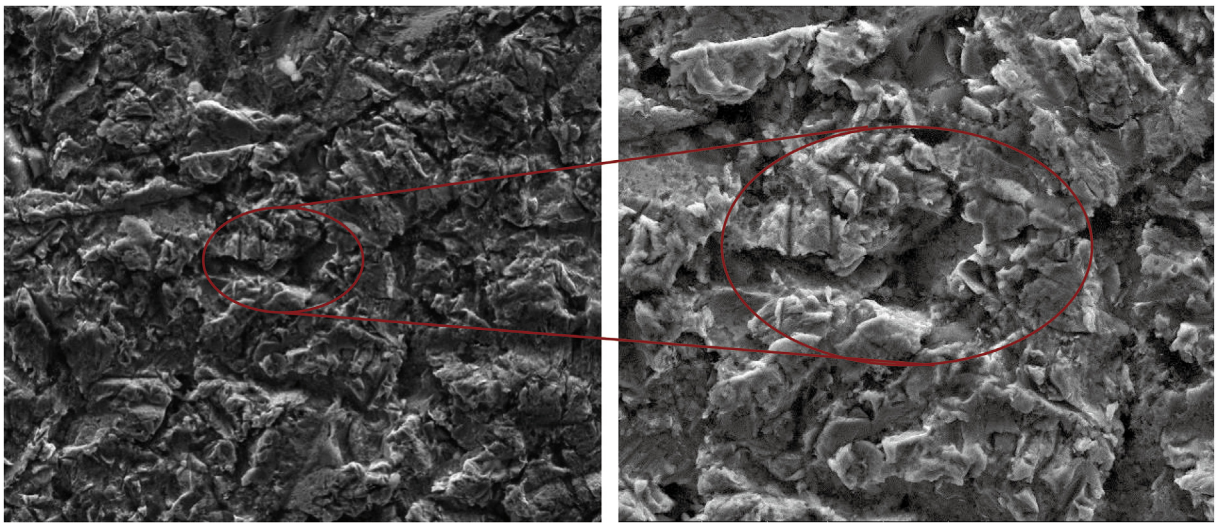

Fig. A4. Surface morphology of L245 carbon steel at 60° (type I particle).

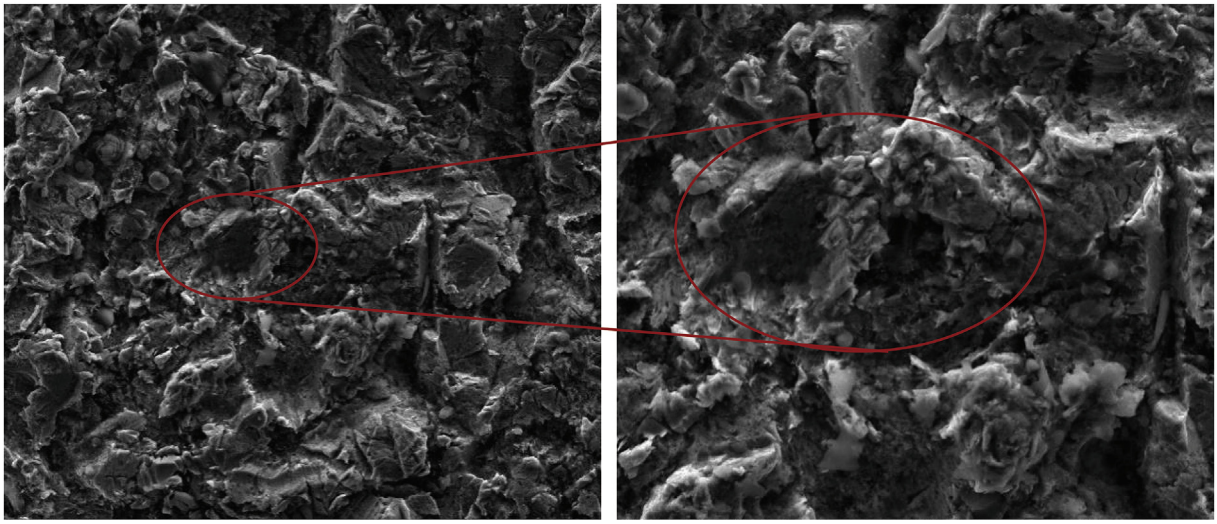

Fig. A5. Surface morphology of L245 carbon steel at 75° (type I particle).

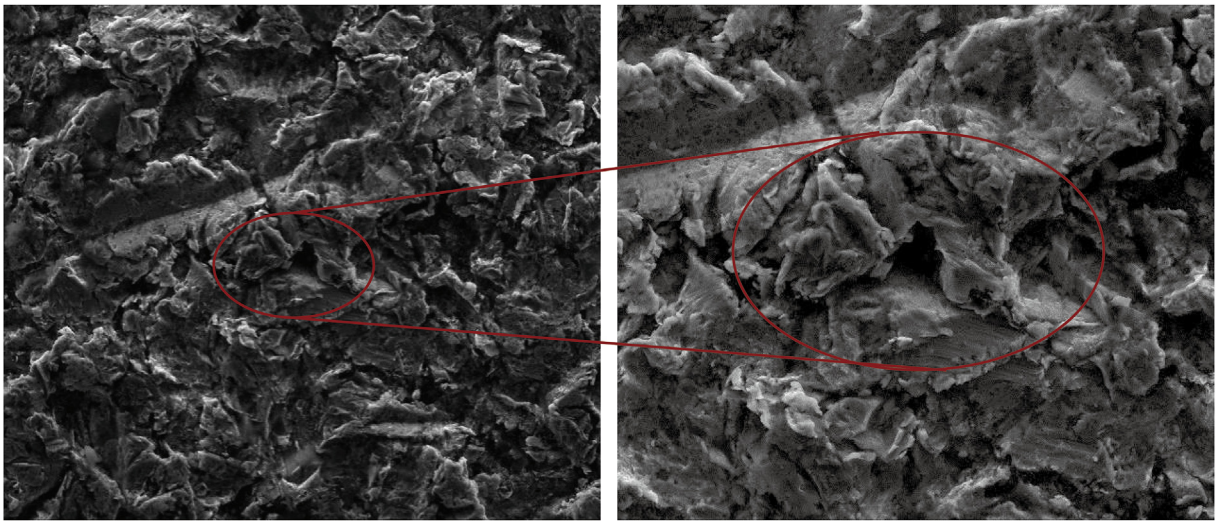

Fig. A6. Surface morphology of L245 carbon steel at 90° (type I particle).

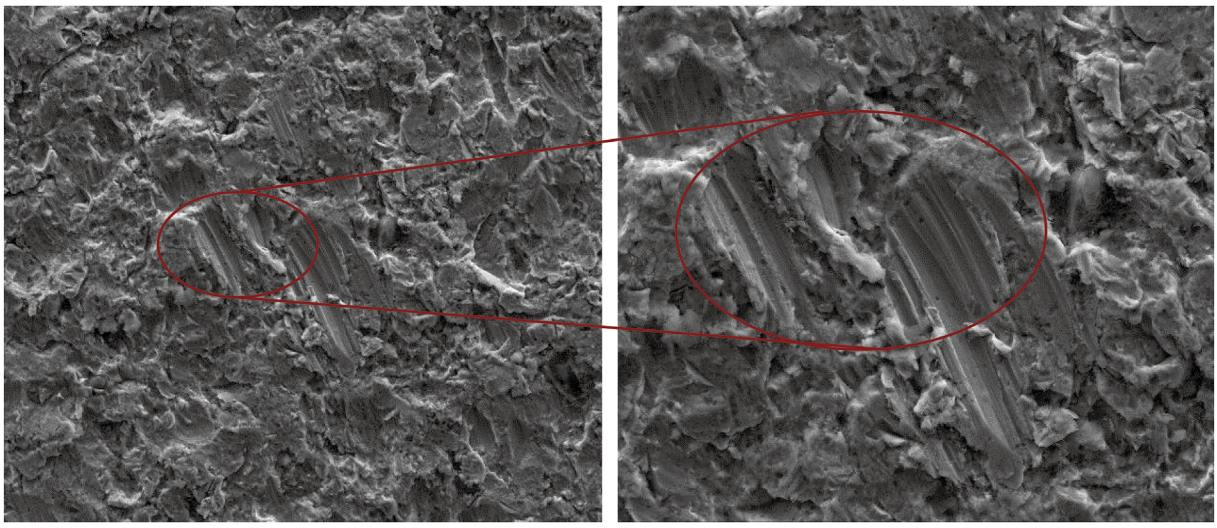

Fig. A7. Surface morphology of L245 carbon steel at 15° (type II particle).

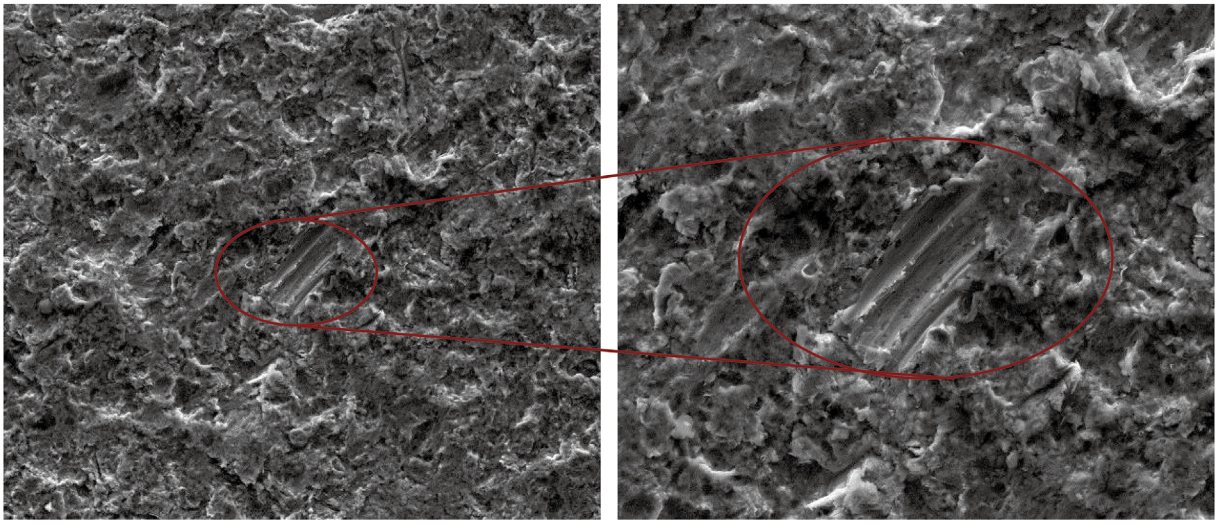

Fig. A8. Surface morphology of L245 carbon steel at 30° (type II particle).

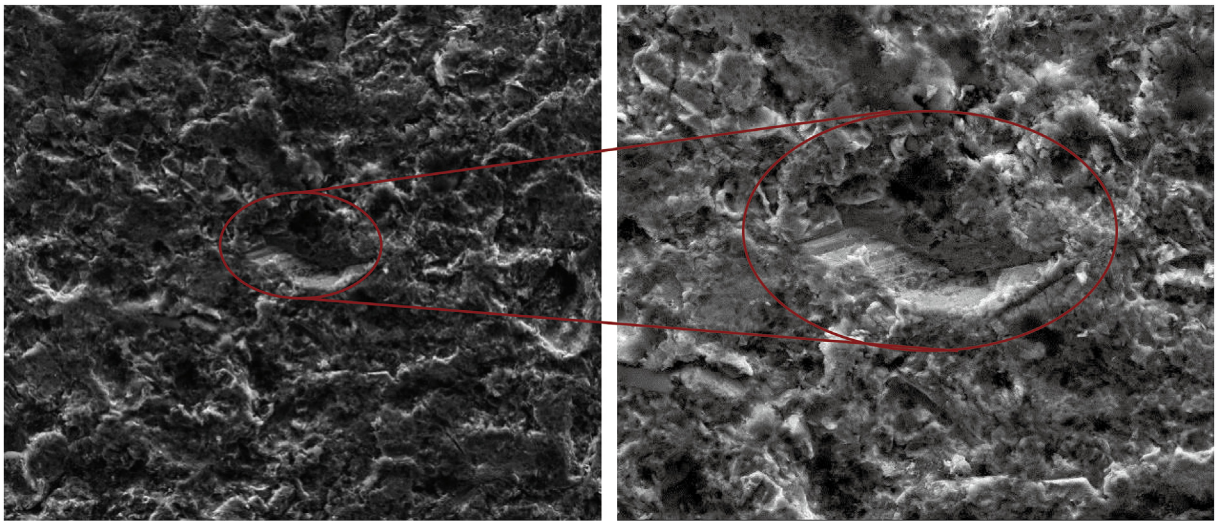

Fig. A9. Surface morphology of L245 carbon steel at 45° (type II particle).

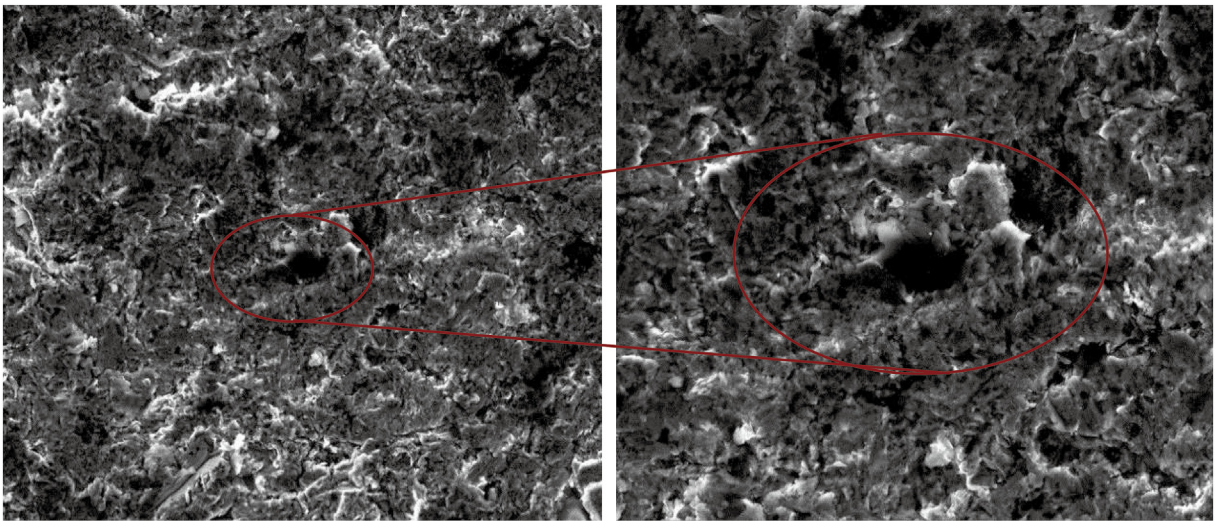

Fig. A10. Surface morphology of L245 carbon steel at 60° (type II particle).

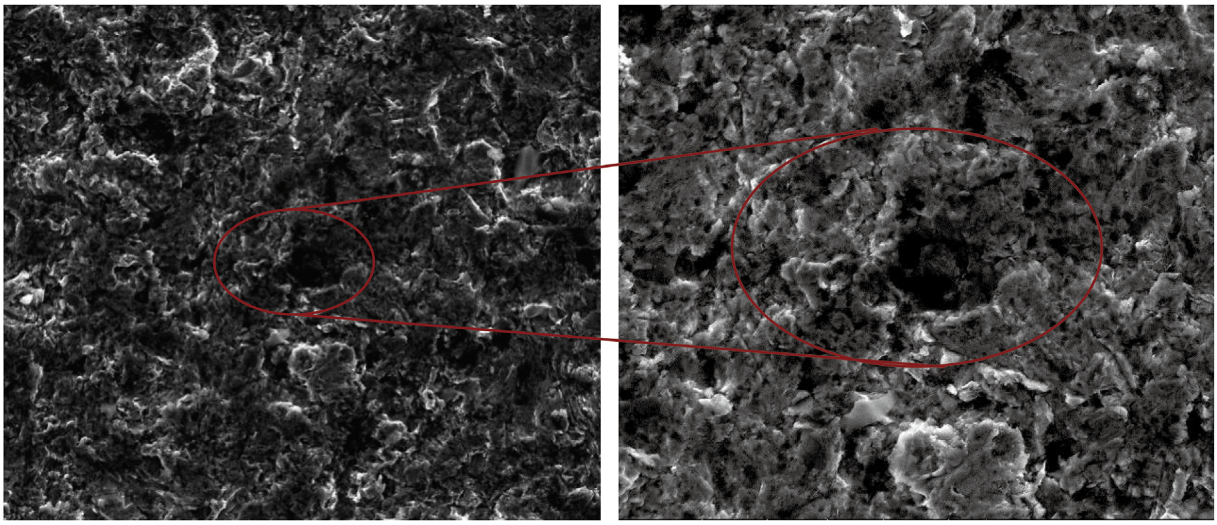

Fig. A11. Surface morphology of L245 carbon steel at 75° (type II particle).

References

Abduljabbar, A., Mohyaldinn, M., Younis, O., Alghurabi, A., 2021. A numerical CFD investigation of sand screen erosion in gas wells: effect of fine content and particle size distribution. J. Nat. Gas Sci. Eng. 95, 104228. https://doi.org/10.1016/j.jngse.2021.104228.

Ahlert, K.R., 1994. Effects of Particle Impingement Angle and Surface Wetting on Solid Particle Erosion of AISI 1018 Steel.

Alghurabi, A., Mohyaldinn, M., Jufar, S., Younis, O., Abduljabbar, A., Azuwan, M., 2021. CFD numerical simulation of standalone sand screen erosion due to gas-sand flow. J. Nat. Gas Sci. Eng. 85, 103706. https://doi.org/10.1016/j.jngse.2020.103706.

Arabnejad, H., Shirazi, S.A., McLaury, B.S., Subramani, H.J., Rhyne, L.D., 2015. The effect of erodent particle hardness on the erosion of stainless steel. Wear 332–333, 1098–1103. https://doi.org/10.1016/j.wear.2015.01.017.

Bilal, F.S., Sedrez, T.A., Shirazi, S.A., 2021. Experimental and CFD investigations of 45 and 90 degrees bends and various elbow curvature radii effects on solid particle erosion. Wear 476, 203646. https://doi.org/10.1016/j.wear.2021.203646.

Bitter, J.G.A., 1963a. A study of erosion phenomena part II. Wear 6, 169–190. https://doi.org/10.1016/0043-1648(63)90073-5.

Bitter, J.G.A., 1963b. A study of erosion phenomena part I. Wear 6, 5–21. https://doi.org/10.1016/0043-1648(63)90003-6.

Finnie, I., 1960. Erosion of surfaces by solid particles. Wear 3, 87–103. https://doi.org/10.1016/0043-1648(60)90055-7.

Hong, B., Li, X., Li, Y.B., Li, Y., Yu, Y., Wang, Y., Gong, J., Ai, D., 2021a. Numerical simulation of elbow erosion in shale gas fields under gas-solid two-phase flow. Energies 14. https://doi.org/10.3390/en14133804.

Hong, B., Li, X., Song, S., Chen, S., Zhao, C., Gong, J., 2020. Optimal planning and modular infrastructure dynamic allocation for shale gas production. Appl. Energy 261, 114439. https://doi.org/10.1016/j.apenergy.2019.114439.

Hong, B., Li, Y., Li, X., Ji, S., Yu, Y., Fan, D., Qian, Y., Guo, J., Gong, J., 2021b. Numerical simulation of gas-solid two-phase erosion for elbow and tee pipe in gas field. Energies 14. https://doi.org/10.3390/en14206609.

Islam, M.A., Farhat, Z.N., 2014. Effect of impact angle and velocity on erosion of API X42 pipeline steel under high abrasive feed rate. Wear 311, 180–190. https://doi.org/10.1016/j.wear.2014.01.005.

Javaheri, V., Porter, D., Kuokkala, V.-T., 2018. Slurry erosion of steel – review of tests, mechanisms and materials. Wear 408–409, 248–273. https://doi.org/10.1016/j.wear.2018.05.010.

Jia, W., Zhang, Y., Li, C., Luo, P., Song, X., Wang, Y., Hu, X., 2021. Experimental and numerical simulation of erosion-corrosion of 90° steel elbow in shale gas pipeline. J. Nat. Gas Sci. Eng. 89, 103871. https://doi.org/10.1016/j.jngse.2021.103871.

Kang, R., Liu, H., 2020. An integrated model of predicting sand erosion in elbows for multiphase flows. Powder Technol. 366, 508–519. https://doi.org/10.1016/j.powtec.2020.02.072.

Lin, N., Arabnejad, H., Shirazi, S.A., McLaury, B.S., Lan, H., 2018. Experimental study of particle size, shape and particle flow rate on Erosion of stainless steel. Powder Technol. 336, 70–79. https://doi.org/10.1016/j.powtec.2018.05.039.

Lin, N., Lan, H., Xu, Y., Dong, S., Barber, G., 2015. Effect of the gas-solid two-phase flow velocity on elbow erosion. J. Nat. Gas Sci. Eng. 26, 581–586. https://doi.org/10.1016/j.jngse.2015.06.054.
Liu, H., Zhou, Z., Liu, M., 2015. A probability model of predicting the sand erosion profile in elbows for gas flow. Wear 342–343, 377–390. https://doi.org/10.1016/j.wear.2015.09.012.
Mansouri, A., Arabnejad, H., Shirazi, S.A., McLaury, B.S., 2015. A combined CFD/experimental methodology for erosion prediction. Wear 332–333, 1090–1097. https://doi.org/10.1016/j.wear.2014.11.025.
Nandre, B.D., Desale, G.R., 2018. Study the effect of impact angle on slurry erosion wear of four different ductile materials. Mater. Today Proc. 5, 7561–7570. https://doi.org/10.1016/j.matpr.2017.11.428.
Nguyen, Q.B., Nguyen, V.B., Lim, C.Y.H., Trinh, Q.T., Sankaranarayanan, S., Zhang, Y.W., Gupta, M., 2014. Effect of impact angle and testing time on erosion of stainless steel at higher velocities. Wear 321, 87–93. https://doi.org/10.1016/j.wear.2014.10.010.
Nguyen, V.B., Nguyen, Q.B., Zhang, Y.W., Lim, C.Y.H., Khoo, B.C., 2016. Effect of particle size on erosion characteristics. Wear 348–349, 126–137. https://doi.org/10.1016/j.wear.2015.12.003.
NovellettoRicardo, G.A., Sommerfeld, M., 2020. Experimental evaluation of surface roughness variation of ductile materials due to solid particle erosion. Adv. Powder Technol. 31, 3790–3816. https://doi.org/10.1016/j.apt.2020.07.023.
Oka, Y.I., Mihara, S., Yoshida, T., 2009. Impact-angle dependence and estimation of erosion damage to ceramic materials caused by solid particle impact. Wear 267, 129–135. https://doi.org/10.1016/j.wear.2008.12.091.
Oka, Y.I., Okamura, K., Yoshida, T., 2005. Practical estimation of erosion damage caused by solid particle impact: Part 1: effects of impact parameters on a predictive equation. Wear 259, 95–101. https://doi.org/10.1016/j.wear.2005.01.039.
Oka, Y.I., Yoshida, T., 2005. Practical estimation of erosion damage caused by solid particle impact: Part 2: mechanical properties of materials directly associated with erosion damage. Wear 259, 102–109. https://doi.org/10.1016/j.wear.2005.01.040.
Parsi, M., Najmi, K., Najafifard, F., Hassani, S., McLaury, B.S., Shirazi, S.A., 2014. A comprehensive review of solid particle erosion modeling for oil and gas wells and pipelines applications. J. Nat. Gas Sci. Eng. 21, 850–873. https://doi.org/10.1016/j.jngse.2014.10.001.
Peng, W., Cao, X., 2016. Numerical prediction of erosion distributions and solid particle trajectories in elbows for gas–solid flow. J. Nat. Gas Sci. Eng. 30, 455–470. https://doi.org/10.1016/j.jngse.2016.02.008.
Peng, W., Cao, X., Hou, J., Ma, L., Wang, P., Miao, Y., 2021. Numerical prediction of solid particle erosion under upward multiphase annular flow in vertical pipe bends. Int. J. Pres. Ves. Pip. 104427. https://doi.org/10.1016/j.ijpvp.2021.104427.
Solnordal, C.B., Wong, C.Y., Boulanger, J., 2015. An experimental and numerical analysis of erosion caused by sand pneumatically conveyed through a standard pipe elbow. Wear 336–337, 43–57. https://doi.org/10.1016/j.wear.2015.04.017.
Song, X.G., Park, J.H., Kim, S.G., Park, Y.C., 2013. Performance comparison and erosion prediction of jet pumps by using a numerical method. Math. Comput. Model. 57, 245–253. https://doi.org/10.1016/j.mcm.2011.06.040.
Tang, C., Yang, Y.C., Liu, P.Z., Kim, Y.J., 2021. Prediction of abrasive and impact wear due to multi-shaped particles in a centrifugal pump via CFD-DEM coupling method. Energies 14. https://doi.org/10.3390/en14092391.
Veritas, D.N., 2007. Recommended practice RP O501 erosive wear in piping systems. Pract DNV Recomm 4.
Vieira, R.E., Mansouri, A., McLaury, B.S., Shirazi, S.A., 2016. Experimental and computational study of erosion in elbows due to sand particles in air flow. Powder Technol. 288, 339–353. https://doi.org/10.1016/j.powtec.2015.11.028.
Wang, K., Li, X., Wang, Y., He, R., 2017. Numerical investigation of the erosion behavior in elbows of petroleum pipelines. Powder Technol. 314, 490–499. https://doi.org/10.1016/j.powtec.2016.12.083.
Wang, Q., Huang, Q., Wang, N., Wen, Y., Ba, X., Sun, X., Zhang, J., Karimi, S., Shirazi, S.A., 2021. An experimental and numerical study of slurry erosion behavior in a horizontal elbow and elbows in series. Eng. Fail. Anal. 130, 105779. https://doi.org/10.1016/j.engfailanal.2021.105779.
Wang, Z., Zhang, J., Shirazi, S.A., Dou, Y., 2019. Predicting erosion in a non-Newtonian shear-thinning jet flow with validated CFD models from PIV and PTV measurements. Wear 426–427, 501–506. https://doi.org/10.1016/j.wear.2018.12.027.
Wong, C.Y., Solnordal, C., Swallow, A., Wu, J., 2013. Experimental and computational modelling of solid particle erosion in a pipe annular cavity. Wear 303, 109–129. https://doi.org/10.1016/j.wear.2013.02.018.
Xie, Z., Cao, X., Fu, C., Zhang, J., Sun, X., Wu, C., Zhao, X., 2021. Experimental study on the repeated impact of sharp particles on metal surface. Wear 474–475, 203716. https://doi.org/10.1016/j.wear.2021.203716.
Zhang, P., Zheng, S., Jing, J., Zhou, Y., Li, Q., Wang, K., Lv, N., Sun, N., 2015. Surface erosion behavior of an intrusive probe in pipe flow. J. Nat. Gas Sci. Eng. 26, 480–493. https://doi.org/10.1016/j.jngse.2015.05.037.
Zhang, Y., Reuterfors, E.P., McLaury, B.S., Shirazi, S.A., Rybicki, E.F., 2007. Comparison of computed and measured particle velocities and erosion in water and air flows. Wear 263, 330–338. https://doi.org/10.1016/j.wear.2006.12.048.
Zheng, S., Luo, M., Xu, K., Li, X., Bie, Q., Liu, Y., Yang, H., Liu, Z., 2019. Case study: erosion of an axial flow regulating valve in a solid-gas pipe flow. Wear 434–435, 202952. https://doi.org/10.1016/j.wear.2019.202952.